

In the previous chapter the importance of the escape energy, C_3 , was highlighted and how it was used to calculate launcher performance. In this chapter we take a closer look at C_3 values for transfers to different planets. We'll limit this to a 10-year period of 2020–2030 however the values of this range should be a good indication of other periods as well.

2.1 Positions of the Planets

Without knowing where planets are located in space, it will be impossible to create a trajectory between them. Mathematical formulas exist, which can be used to determine the position of a planet as function of the date. The Horizon program of JPL (Jet Propulsion Laboratory, see [1]) is a useful tool to give the most accurate positions of celestial bodies currently available. This ephemeris module is also implemented in the Satellite Tool Kit software (download from [2]). However when positions are given, they relate to a certain coordinate system consisting of an origin and three axes. As origin, typical choices are the Sun, the barycenter of the Solar System (which is actually situated inside the Sun), or the Earth.

In terms of axes two systems are mostly used for planet positions: the ecliptic plane and the ICRF (International Celestial Reference Frame) system. The ecliptic plane is simply the plane of the Earth's orbit around the Sun. It was named ecliptic because a solar eclipse can only occur when the Moon crosses this plane. The plane moves over time so it should be accompanied by an epoch and typically the first of January of the year 2000 is used. While the Earth moves within the ecliptic frame, the other planets are located near this plane: the orbits of the other planets are not largely inclined with respect to the ecliptic plane. The ecliptic plane intersects the Earth's equator plane by a line between two imaginary points: the vernal equinox and the autumn equinox. This allows for a definition of axes based on the ecliptic plane: the X and Y axes are located within the ecliptic plane with the X-axis pointed to the vernal equinox along the intersection of

the ecliptic plane with the Earth equator plane, and the Z-axis perpendicular to the ecliptic plane. The Y-axis makes up for a right-handed axes system (Figs. 2.1 and 2.2).

Even though a coordinate system based on the ecliptic plane seems the obvious choice as a reference system for planet positions, often the ICRF is used. This frame uses the Solar System barycenter as origin, and the Earth's equator as reference plane. The X and Y-axis lie within the equator plane with the X-axis pointing towards the vernal equinox on January 1st 2000, and the Z-axis points perpendicular to the Earth's equator plane on January 1st 2000 (i.e. towards the North Pole). The Y-axis makes up for a right-handed axes system.

One advantage of using the ICRF frame to calculate planet positions, is that we can then calculate the trajectories within this frame, and immediately know the declination of the escape vector, as the declination is also defined with respect to the equator plane.

The average distance from the Sun to the Earth is called Astronomical Unit (AU), and is equal to 149,597,870 km, almost 150 million km. Table 2.1 gives an overview of the average distances from all planets to the Sun, measured in AU. Pluto, which was considered a planet until recently, is included as well, along with the asteroid Apophis.

Note that most planet orbits are slightly elliptical. Therefore the actual distance to the Sun for a specific point in time may be quite different from the average distance. Celestial bodies like Apophis and Pluto are more elliptical than the planets: the shortest distance from the Sun to Apophis (or 'Perihelion') is 0.75 AU and the largest distance ('Aphelion') is 1.1 AU.

Planetary trajectories are only feasible if the planets that are touching the trajectory (like the departure planet and the arrival planet) are correctly aligned. Figure 2.3 shows the positions of Earth and Mars at time of launch in July 2020. At this time, Earth and Mars are correctly aligned for a transfer. If this launch window is missed, we need to wait for the next time that the planets have a similar alignment (due

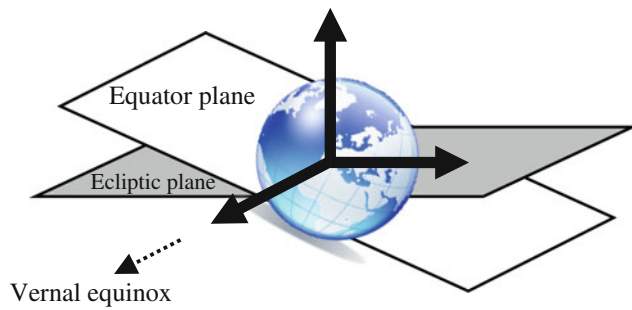


Fig. 2.1 Definition of axes based on the ecliptic plane

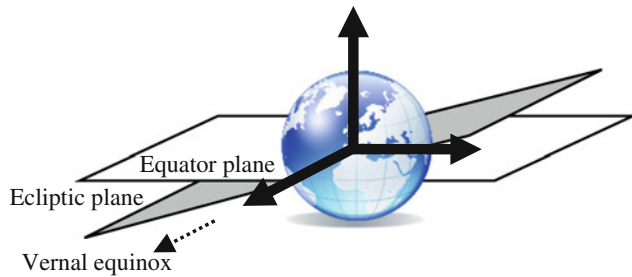


Fig. 2.2 Definition of ICRF axes based on the equator plane

Table 2.1 Average distances to the Sun and synodic period for all planets, Pluto and Apophis

Planet or celestial body	Average distance to Sun [AU]	Synodic period [year]
Mercury	0.4	0.32
Venus	0.7	1.6
Apophis (Asteroid)	0.9	7.8
Earth	1	–
Mars	1.5	2.1
Jupiter	5	1.1
Saturn	10	1.0
Uranus	20	1.0
Neptune	30	1.0
Pluto	40	1.0

to the fact that the planet orbits are elliptical the new alignment will not be completely the same). The time it takes to be aligned again depends on the relative velocity between the planets.

The time it takes for a celestial body to reappear at the same point in relation to two other objects (of which one is usually the Sun) is called the Synodic Period. Table 2.1 shows the Synodic Period between Earth and the other celestial bodies of the table. We see periods higher than one year for planets that are relatively close to the Earth (and therefore have a small relative velocity), like Mars and Venus, and a Synodic Period of about 1 year for all outer

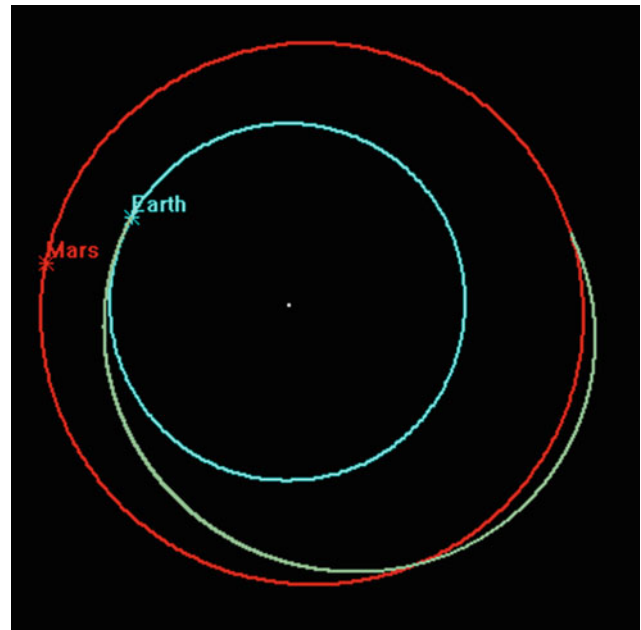


Fig. 2.3 Earth and Mars positions at time of launch in July 2020. The trajectory is shown as an ellipse connecting the two near-circular planet orbits

planets. This means that every year there is a launch opportunity for Jupiter and all planets beyond Jupiter, while missions to Mars are possible only once every two years.

2.2 Devising Trajectories to Other Planets

So how do we calculate a trajectory from one planet to the other? The easiest solution to this is to follow this sequence:

1. Determine the position of the departure planet at time T_1 . We call this position R_1 .
2. Determine the position of the arrival planet at time T_2 . We call this position R_2 .
3. Find a trajectory starting at position R_1 at time T_1 and ending at position R_2 at time T_2 . In other words: the travel time is: $(T_2 - T_1)$.

The first two actions can be determined as discussed the previous chapter: using JPL's Horizon program we can get the position vector within a Sun-centered ICRF frame for any planet at any time.

The third action is more difficult and can only be found by solving what is called Lambert's problem, see Fig. 2.4. This 'Lambert solver' basically does three steps:

1. It is assumed that the connecting trajectory lies in a plane defined by three points: R_1 , R_2 and the center of attraction (in this case, the Sun).

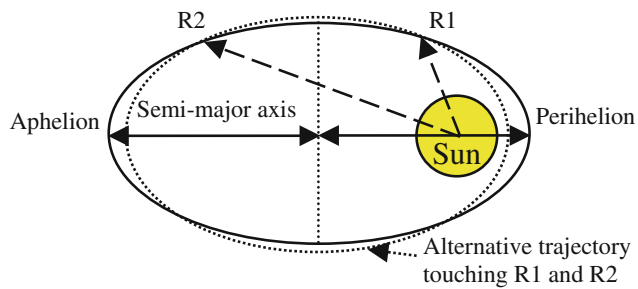


Fig. 2.4 Devising a trajectory between two points

2. It then determines an elliptic trajectory that touches both R1 and R2, based on an assumed semi-major axis of this trajectory.
3. Since this assumed semi-major axis does not give exactly a transfer time from R1 to R2 equal to $(T_2 - T_1)$, an iteration on the semi-major axis is performed until the transfer time is exactly $(T_2 - T_1)$.

The semi-major axis is the distance between the center of the trajectory ellipse and the edge of the ellipse. Usually two solutions exist: a prograde (in this case, anti-clockwise) and a retrograde (clockwise) solution. Since all planets move in an anti-clockwise direction, almost all transfers are prograde/anti-clockwise. The mathematical foundations of Lambert's problem can be found in literature. In this book, it is important to know the main implication of this problem:

A trajectory is only found based on a given transfer time using the Lambert solver.

So does this mean that for any departure date at one planet and arrival date at the other planet, we can find a trajectory? In principle, yes. However, the output of the Lambert solver is:

1. Which velocity you need at position R1 at time T1 to reach position R2 at time T2 (called the departure 'infinite velocity')
2. With which velocity do you arrive at R2 (called the arrival 'infinite velocity')

We know from Sect. 1.2 that C_3 is the square of the infinite velocity, so the Lambert solver gives us the departing C_3 and the arrival C_3 . We also know that the lower the departure C_3 , the more mass we can launch. So we clearly want to have low C_3 's in order for our trajectory to be physically feasible (a solution to Lambert's problem that leads to a departure C_3 of $500 \text{ km}^2/\text{s}^2$ is beyond the reach of any launcher, for example).

In practice, what we want to minimize is the velocity change, or ΔV . Often mission analysts minimize the escape infinite velocity and the total ΔV required for orbit changes.

For a direct transfer, we would try to minimize the infinite velocity, which is the square root of the escape C_3 , plus the planet orbit insertion ΔV , which is a function of the arrival C_3 . This leads to the core of interplanetary trajectory design:

Find the trajectory that gives a minimal total ΔV .

How? We repeat the inputs of Lambert's problem: time T1 and time T2. So finding the optimal transfer means finding the optimal departure time T1 and the optimal arrival time T2!

An optimization sequence could look like this:

Perform a loop in time T1 for all dates in selected launch year

- For this time T1, determine the position of the departure planet: R1
- Perform a loop in time T2 for all dates in selected arrival year
 - For this time T2, determine the position of the arrival planet: R2
 - Using a Lambert solver, calculate a trajectory between R1 and R2 for which the transfer time is $(T_2 - T_1)$
 - Based on the departure and arrival infinite velocities, calculate the departure and arrival C_3
 - From the departure and arrival C_3 , calculate the total ΔV
 - If the ΔV of this solution is lower than any previously found solution, remember the times T1 and T2
- End loop in time T2

End loop in time T1

The solution is the combination T1, T2 that lead to the lowest ΔV

The next chapter shows the results of an optimization as stated above, for all planets.

2.3 Launch Windows and C_3 Values for Direct Transfers to the Planets

For the celestial bodies shown in Table 2.1, an optimization as shown in the previous section was performed using the following rules:

- The Earth escape infinite velocity plus orbit insertion ΔV was minimized
- For inner planets, a final orbit altitude of 500 km was used
- For outer planets, a final orbit altitude equal to planet radius was used
- A maximum transfer time of 10 years was applied (longer transfer times are unlikely to be accepted by project managers)

Table 2.2 Solutions for a direct transfer from Earth to Mercury

Year	Launch date	Arrival date	C3 launch [km^2/s^2]	C3 arrival [km^2/s^2]	Declination [$^\circ$]	Transfer time [yr]
2020	6-Nov-20	7-Mar-21	47.7	142.7	4.6	0.33
2021	31-Oct-21	21-Feb-22	43.5	146.2	-8.1	0.31
2022	13-Oct-22	5-Feb-23	44.0	162.6	-22.1	0.31
2023	27-Sep-23	21-Jan-24	48.6	171.8	-26.8	0.32
2024	8-Sep-24	3-Jan-25	55.8	173.3	-31.9	0.32
2025	21-Aug-25	17-Dec-25	65.5	169.3	-33.7	0.32
2026	9-Nov-26	17-Mar-27	54.1	143.3	11.7	0.35
2027	6-Nov-27	1-Mar-28	44.9	140.8	0.7	0.32
2028	24-Oct-28	14-Feb-29	43.1	153.4	-15.0	0.31
2029	5-Oct-29	29-Jan-30	46.1	166.8	-25.3	0.32
2030	18-Sep-30	13-Jan-31	51.6	172.4	-30.3	0.32

Table 2.3 Solutions for a direct transfer from Earth to Mercury, constrained to 28.5° launch declination

Year	Launch date	Arrival date	C3 launch [km^2/s^2]	C3 arrival [km^2/s^2]	Declination [$^\circ$]	Transfer time [yr]
2024	12-Sep-24	5-Jan-25	54.7	180.7	-28.5	0.31
2025	30-Aug-25	21-Dec-25	62.1	191.5	-27.8	0.31
2030	20-Sep-30	14-Jan-31	51.2	174.4	-28.4	0.32

- A maximum absolute launch declination of 51.8° was applied (higher declinations are not achievable by any of the launchers mentioned in Sect. 1.6.4).

The following sections give the optimal solutions for each year in the 2020–2030 timeframe. The solutions contain launch date and C3, arrival date and C3, launch declination and transfer time.

A ‘launch window’ is often defined taking a three-week period surrounding the optimal launch date found. This means that the C3 value changes depending on the day in the launch window, and therefore the allowable launch mass. Often a launch occurs on the first or second day in the window, which is typically a worse solution than the optimal solution that probably lies somewhere in the middle of the launch window. A mission analyst would need to calculate a trajectory for each day in the launch window, and a system engineer would need to assume the worst-case scenario within that launch window. An alternative is to use the optimal solution only and apply a margin. For example, a 1.5 % margin can be put on the launch mass of the optimal solution to account for the other dates in the launch window.

2.3.1 Direct Transfer to Mercury

Table 2.2 shows the results for transfers to Mercury. Note that according to Table 2.1 we should have multiple possibilities per year. The table shows only 1 solution per year; the one leading to the lowest ΔV .

We also see that there are three years: 2024, 2025 and 2030 where the launch declination is higher than 28.5° . This means that this launch would be incompatible with a launch from Cape Canaveral without performing an expensive inclination change during the launch. We can constrain the declination and re-optimize for these cases: the results are shown in Table 2.3; the constraint leads different dates and a higher arrival C3.

Figure 2.5 shows the departure and arrival C3 in graphical form.

Note how high the arrival C3 is. This would lead to huge insertion ΔV s. The arrival C3 can only be minimized by implementing swing-bys and/or Deep-Space Maneuvers within the trajectory. Figure 2.6 shows a typical Earth-Mercury trajectory.

2.3.2 Direct Transfer to Venus

Table 2.4 shows the results for transfers to Venus. Since we know from Table 2.1 that the Synodic Period is 1.6 years, there are years where there is no short-transfer solution for a transfer to Venus. A long transfer is then the result (>1 year), which allows the spacecraft to ‘wait in orbit’ for the next arrival possibility. In 2025 no solution was found.

We also see that there are two years: 2020 and 2028 where the launch declination is higher than 28.5° . Again, we constrained the declination and re-optimized for these cases: the results are shown in Table 2.5; the constraint leads different dates and a higher arrival C3.

Fig. 2.5 Departure and arrival C3 for a direct transfer from Earth to Mercury

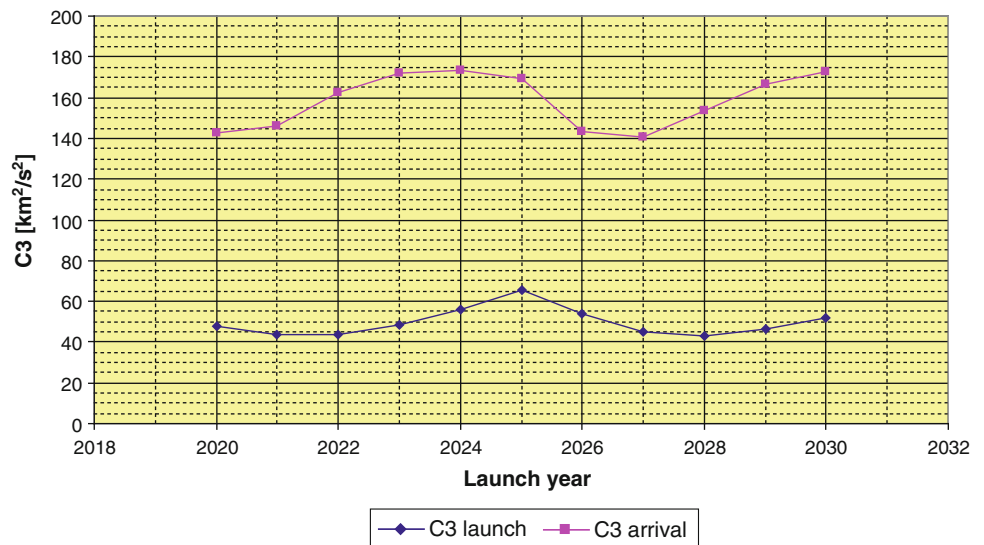


Figure 2.7 shows the departure and arrival C3 in graphical form.

Figure 2.8 shows a typical Earth-Venus trajectory.

ESA's Venus Express mission was launched on 9 November 2005 from Baikonur using a Soyuz-Fregat launcher and arrived at Venus on 11 April 2006 after a 153-day direct transfer (see Fig. 2.9).

Based on ESA's Mars Express platform, launched five years earlier, the 1270 kg Venus Express spacecraft carried 570 kg of propellant for Venus orbit insertion applied using a bi-propellant 400 N engine, and orbit maintenance, applied using small thrusters on the corners of the spacecraft. Communication to Earth was done using a high-gain 1.3 m antenna. Two solar panels covering a total area of 5.8 m^2

provided for 800 W of power at Earth. Figure 2.10 shows an artist's overview of Venus Express.

2.3.3 Direct Transfer to Mars

Table 2.6 shows the results for transfers to Mars. We know from Table 2.1 that the Synodic Period is 2 years, so every other year there is no solution for a transfer to Mars.

Figure 2.11 shows the departure and arrival C3 in graphical form.

Figure 2.12 shows a typical Earth-Mars trajectory.

Practically every mission to Mars uses a direct transfer. NASA's Mars Science Laboratory (MSL) mission is no

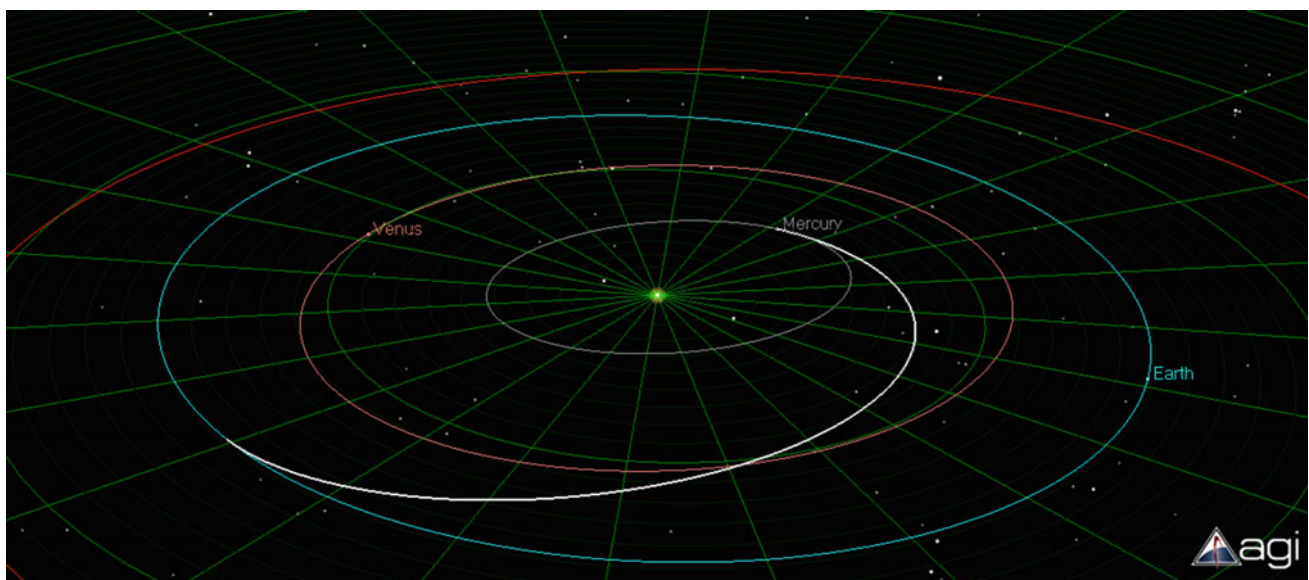


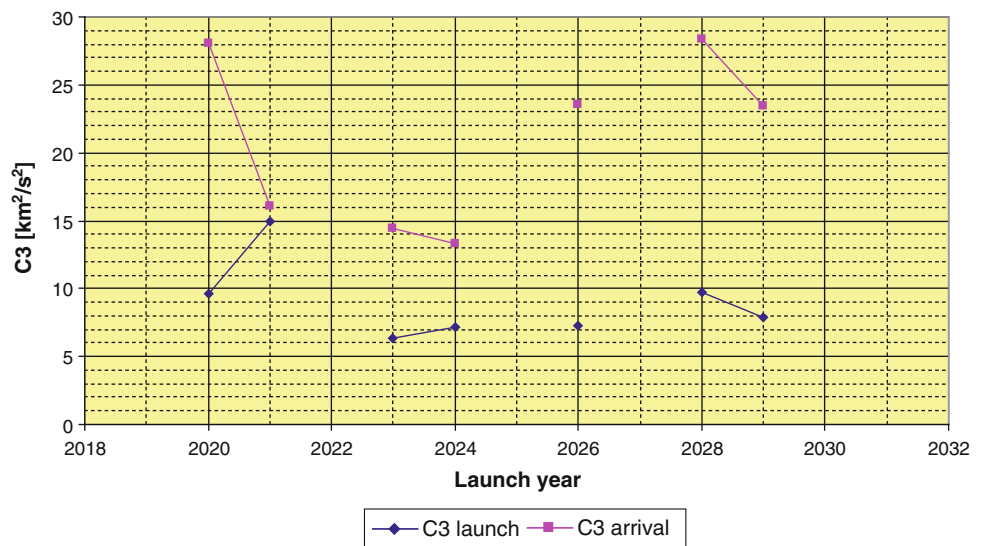
Fig. 2.6 Earth-Mercury trajectory seen from a 3D perspective. Planet positions are shown at time of arrival

Table 2.4 Solutions for a direct transfer from Earth to Venus

Year	Launch date	Arrival date	C3 launch [km^2/s^2]	C3 arrival [km^2/s^2]	Declination [$^\circ$]	Transfer time [yr]
2020	14-Mar-20	5-Sep-20	9.6	28.1	46.6	0.48
2021	2-Nov-21	19-Feb-22	14.9	16.1	13.3	0.30
2022	7-Dec-22	14-Feb-24	7.0	8.8	6.2	1.20
2023	21-May-23	26-Oct-23	6.3	14.4	9.8	0.43
2024	21-Dec-24	7-May-25	7.2	13.3	6.5	0.38
2025						
2026	31-Jul-26	1-Dec-26	7.3	23.6	2.0	0.34
2027	20-Oct-27	9-Jan-29	8.2	25.9	-28.3	1.20
2028	13-Mar-28	3-Sep-28	9.7	28.4	47.9	0.48
2029	26-Oct-29	4-Apr-30	7.9	23.4	-27.8	0.44
2030	5-Dec-30	13-Feb-32	6.7	10.2	-0.7	1.2

Table 2.5 Solutions for a direct transfer from Earth to Venus, constrained to 28.5° launch declination

Year	Launch date	Arrival date	C3 launch [km^2/s^2]	C3 arrival [km^2/s^2]	Declination [$^\circ$]	Transfer time [yr]
2020	1-Apr-20	21-Sep-20	9.2	36.6	28.4	0.47
2028	31-Mar-28	20-Sep-28	9.4	37.6	28.5	0.47

Fig. 2.7 Departure and arrival C3 for a direct transfer from Earth to Venus

exception. Launched on 26 November 2011 by the Atlas V launcher, MSL arrived at Mars on 6 August 2012 when its rover ‘Curiosity’ landed on the surface of Mars, inside the Gale crater. Figure 2.13 shows the trajectory.

2.3.4 Direct Transfer to Jupiter

Table 2.7 shows the results for transfers to Jupiter. We know from Table 2.1 that the Synodic Period for all outer planets is about 1 year, so we find a solution for every year.

We also see that there is one year (2024) where the launch declination is higher than 28.5° . Again, we

constrained the declination and re-optimized for this case: the results are shown in Table 2.8; the constraint leads different dates and a higher arrival C3 but lower launch C3.

Figure 2.14 shows the departure and arrival C3 in graphical form.

Note that the launch C3 is already higher than any launcher can give using a direct injection. Figure 2.15 shows a typical Earth-Jupiter trajectory.

2.3.5 Direct Transfer to Saturn

Table 2.9 shows the results for transfers to Saturn.

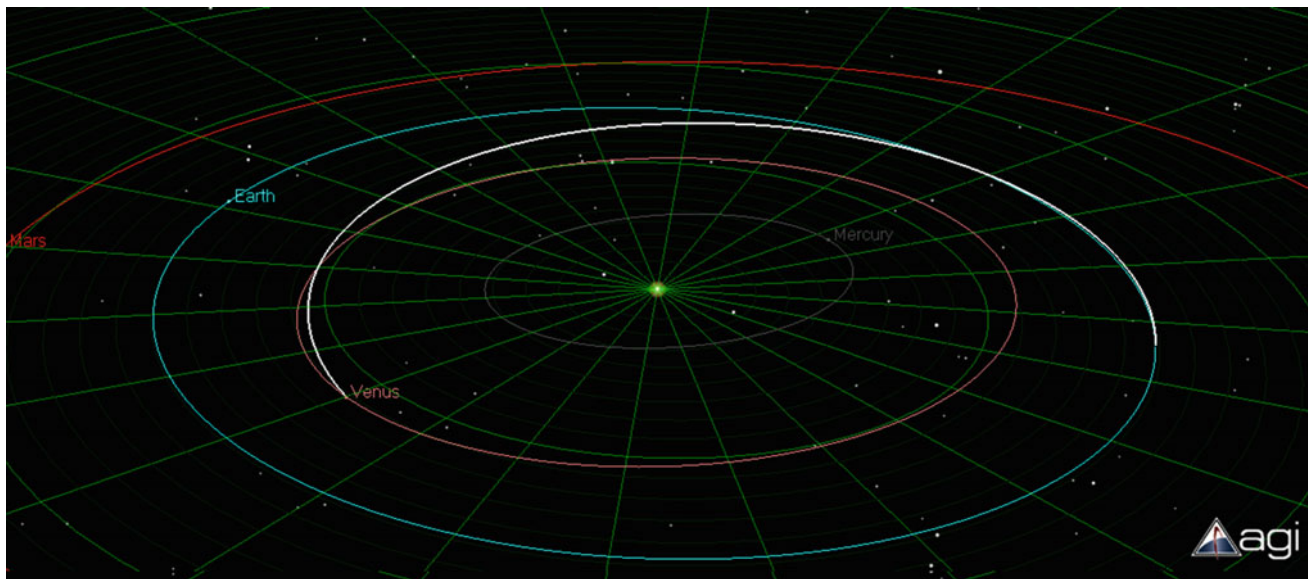


Fig. 2.8 Earth-Venus trajectory seen from a 3D perspective. Planet positions are shown at time of arrival

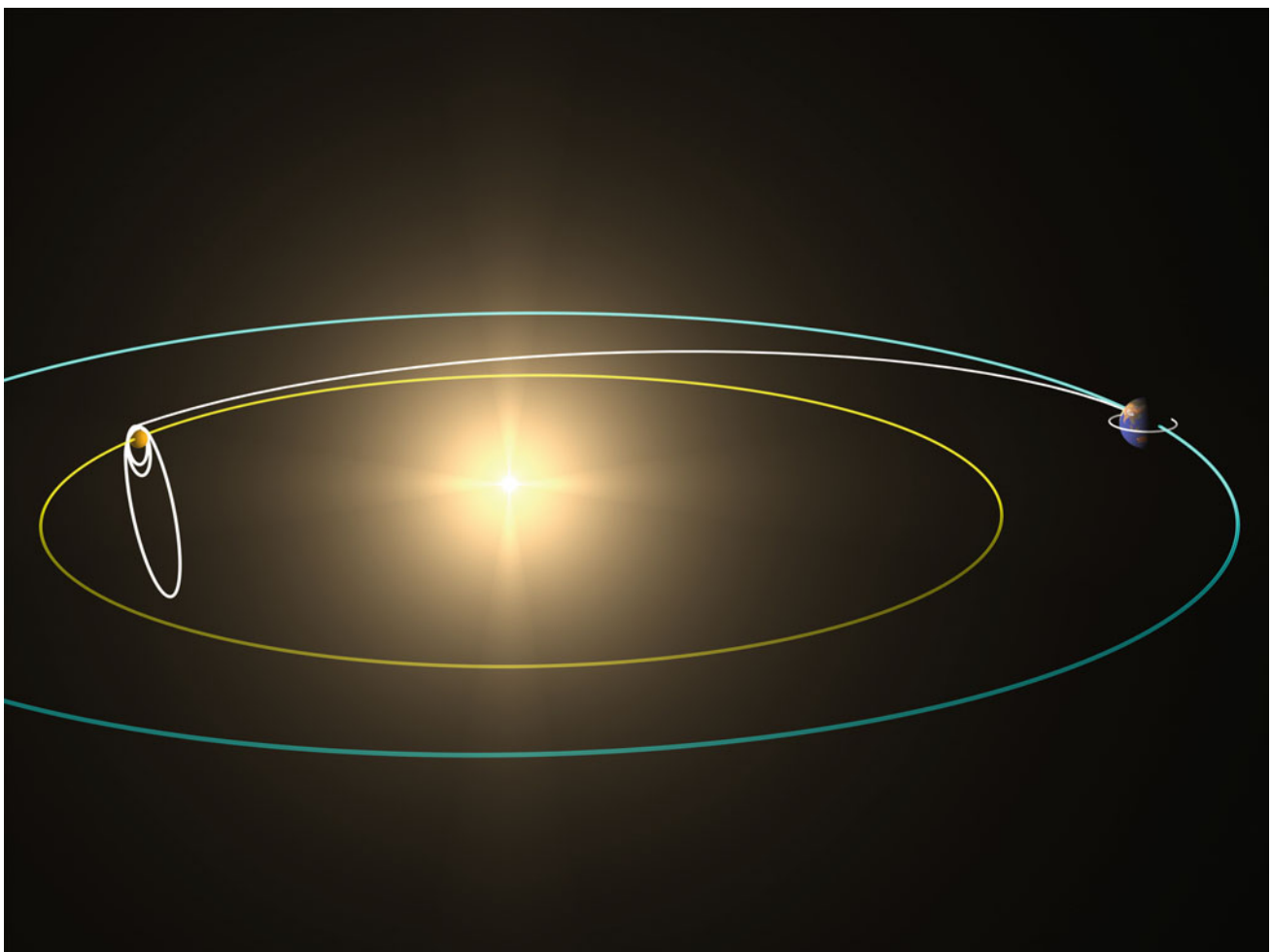


Fig. 2.9 Venus express trajectory. Credits ESA

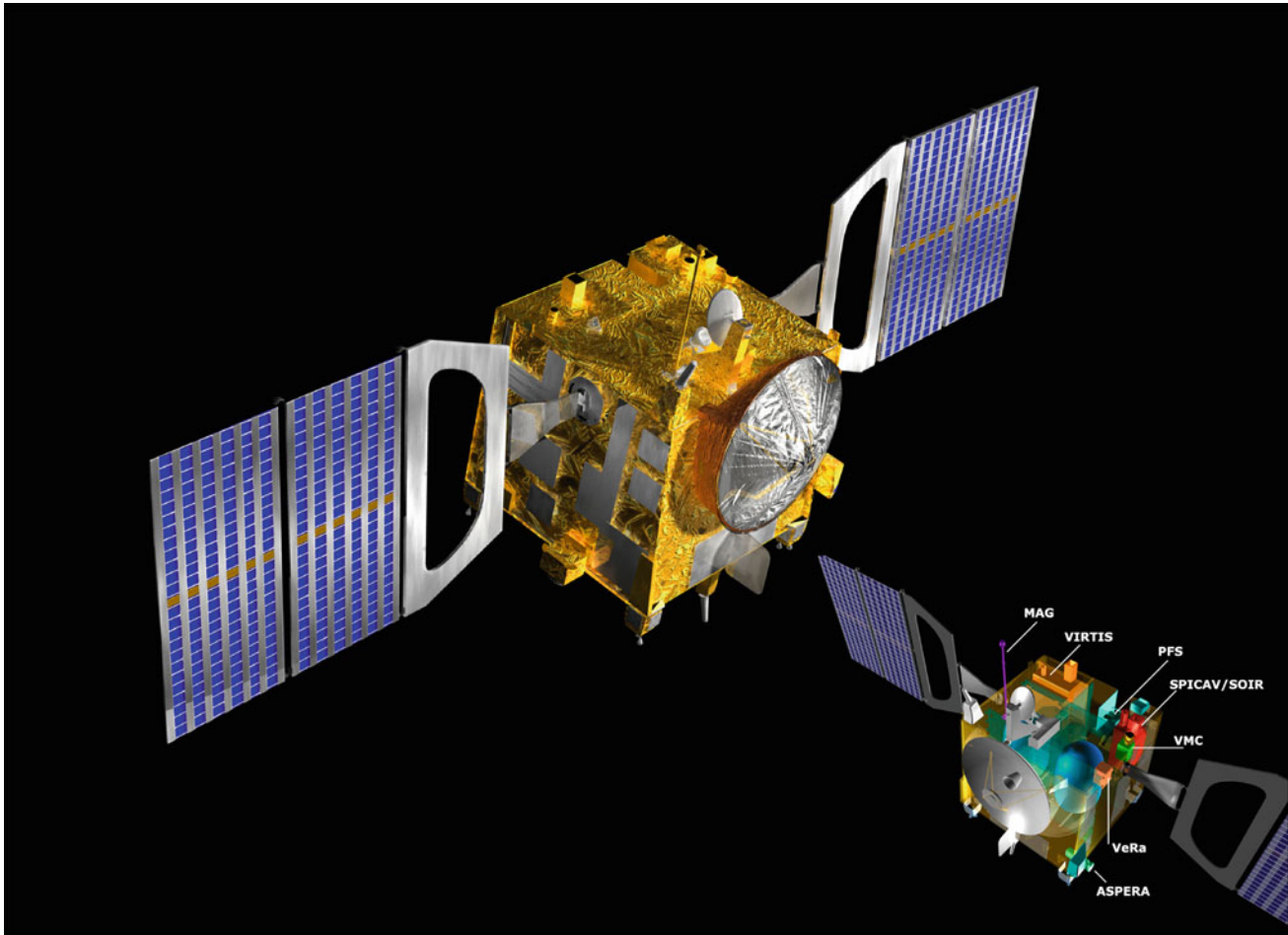


Fig. 2.10 Venus express overview. *Credits ESA*

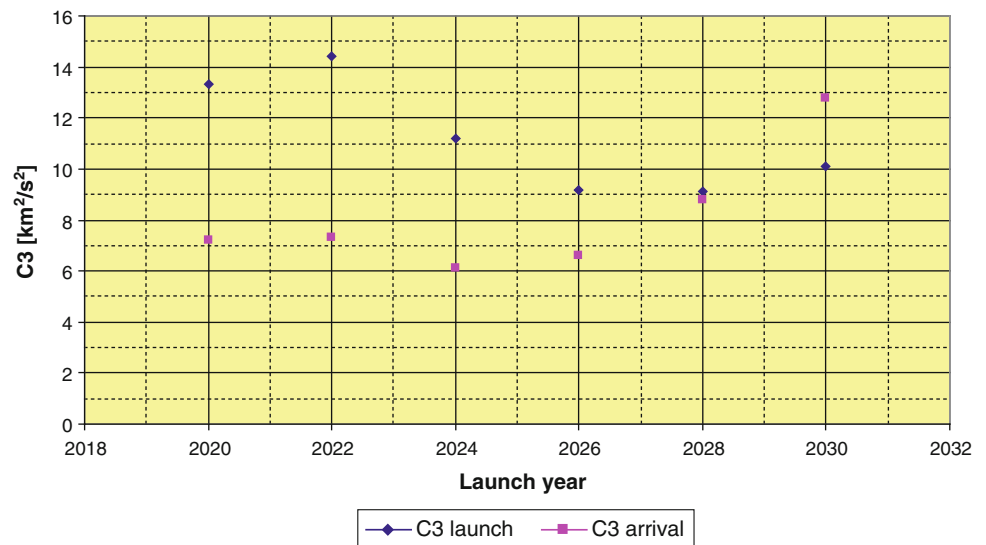
Table 2.6 Solutions for a direct transfer from Earth to Mars

Year	Launch date	Arrival date	C3 launch [km^2/s^2]	C3 arrival [km^2/s^2]	Declination [$^\circ$]	Transfer time [yr]
2020	21-Jul-20	8-Feb-21	13.3	7.2	25.9	0.55
2021						
2022	4-Sep-22	27-Aug-23	14.4	7.3	6.6	0.98
2023						
2024	3-Oct-24	4-Sep-25	11.2	6.1	16.8	0.92
2025						
2026	31-Oct-26	3-Sep-27	9.2	6.6	28.3	0.84
2027						
2028	23-Nov-28	21-Sep-29	9.1	8.8	28.4	0.83
2029						
2030	31-Dec-30	14-Oct-31	10.1	12.8	16.6	0.79

We see that the first five years the launch declination is higher than 28.5° . Again, we constrained the declination and re-optimized for these cases: the results are shown in Table 2.10; the constraint led to different dates and a much higher departure C3. Another outcome was that the

optimized results led to a transfer time of 10 years, equal to the maximum forced transfer time. Since that transfer time would be too long for Saturn (compared to the non-constrained transfers) and it was found that the total ΔV did not change much when decreasing the transfer time from

Fig. 2.11 Departure and arrival C3 for a direct transfer from Earth to Mars



10 to 7 year, a maximum transfer time of 7 years was enforced for these particular cases.

Figure 2.16 shows the departure and arrival C3 in graphical form.

Figure 2.17 shows a typical Earth-Saturn trajectory.

Figure 2.18 shows the departure and arrival C3 in graphical form.

Figure 2.19 shows a typical Earth-Uranus trajectory, constrained to 10 years transfer time.

2.3.6 Direct Transfer to Uranus

Table 2.11 shows the results for transfers to Uranus.

For these cases the maximum transfer constraint of 10 years is clearly active: all cases converged to this maximum transfer time. All transfers are therefore relatively similar; all launching in the June-August timeframe, and all departure and arrival C3's are of the same magnitude.

2.3.7 Direct Transfer to Neptune

Table 2.12 shows the results for transfers to Neptune.

There is a similar behavior to the Uranus cases here: same launch period, same transfer time (10 years) and same C3 values over the decennium.

Figure 2.20 shows the departure and arrival C3 in graphical form.

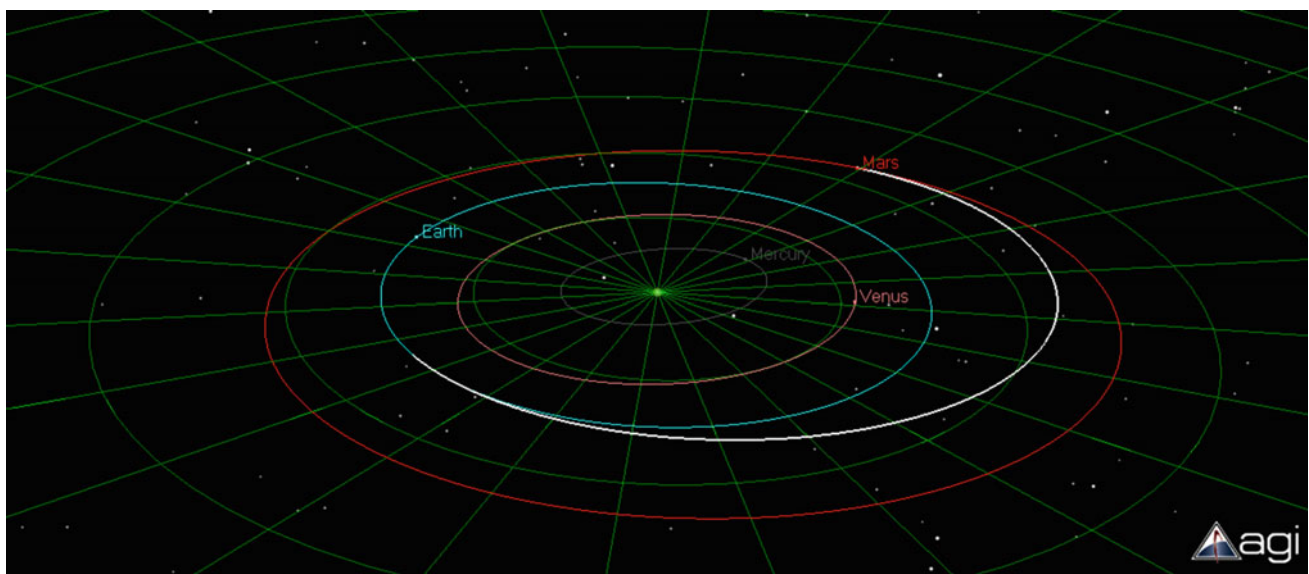


Fig. 2.12 Earth-Mars trajectory seen from a 3D perspective. Planet positions are shown at time of arrival

Fig. 2.13 Mars science
Laboratory trajectory. *Credits*
NASA

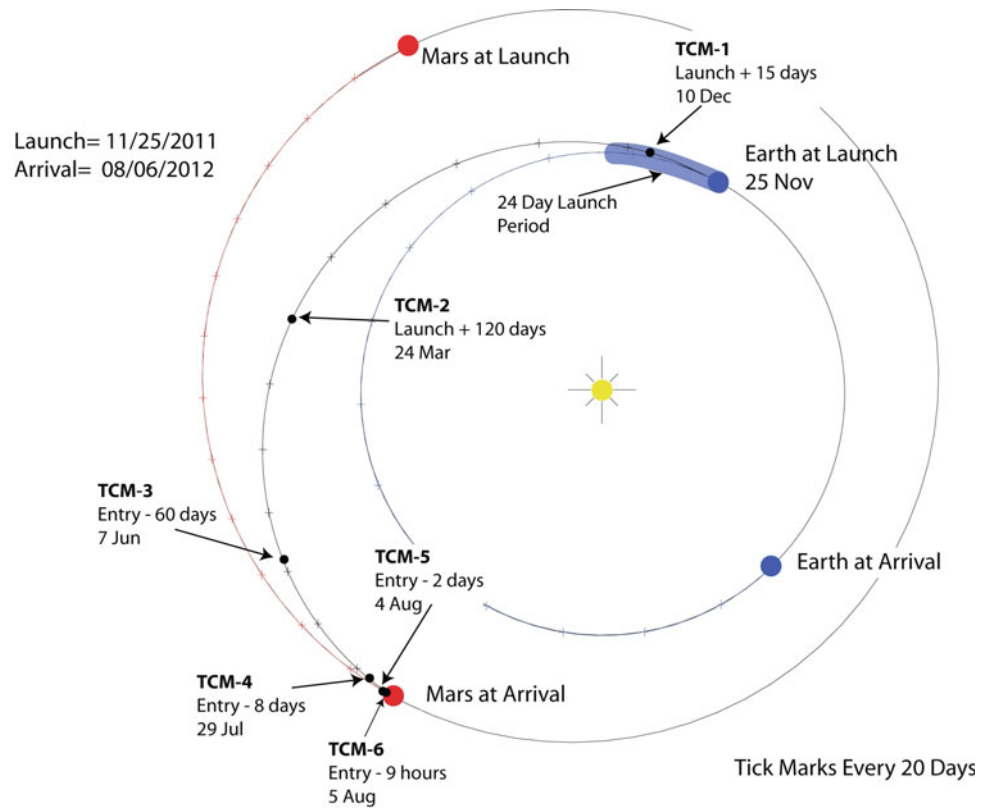


Table 2.7 Solutions for a direct transfer from Earth to Jupiter

Year	Launch date	Arrival date	C3 launch [km^2/s^2]	C3 arrival [km^2/s^2]	Declination [$^\circ$]	Transfer time [yr]
2020	15-Apr-20	28-Nov-23	85.3	52.0	-3.6	3.62
2021	17-May-21	28-Sep-24	83.0	45.0	1.2	3.37
2022	21-Jun-22	28-Jul-25	80.0	37.0	4.0	3.10
2023	17-Jul-23	6-Dec-25	80.6	32.7	13.2	2.39
2024	22-Aug-24	24-Nov-26	87.0	36.3	30.6	2.26
2025	1-Oct-25	30-May-29	89.7	35.5	5.0	3.66
2026	1-Nov-26	31-May-30	85.4	34.8	1.1	3.58
2027	2-Dec-27	29-May-31	79.3	35.5	-1.0	3.49
2028	25-Dec-28	18-Dec-31	75.0	32.4	-3.7	2.98
2029	1-Jan-29	6-Jan-32	77.5	32.8	-1.1	3.01
2030	22-Jan-30	4-Jun-32	77.0	38.6	-18.1	2.37

Table 2.8 Solution for a direct transfer from Earth to Jupiter, constrained to 28.5° launch declination

Year	Launch date	Arrival date	C3 launch [km^2/s^2]	C3 arrival [km^2/s^2]	Declination [$^\circ$]	Transfer time [yr]
2024	22-Aug-24	31-Oct-26	68.9	38.4	28.5	2.19

Fig. 2.14 Departure and arrival C3 for a direct transfer from Earth to Jupiter

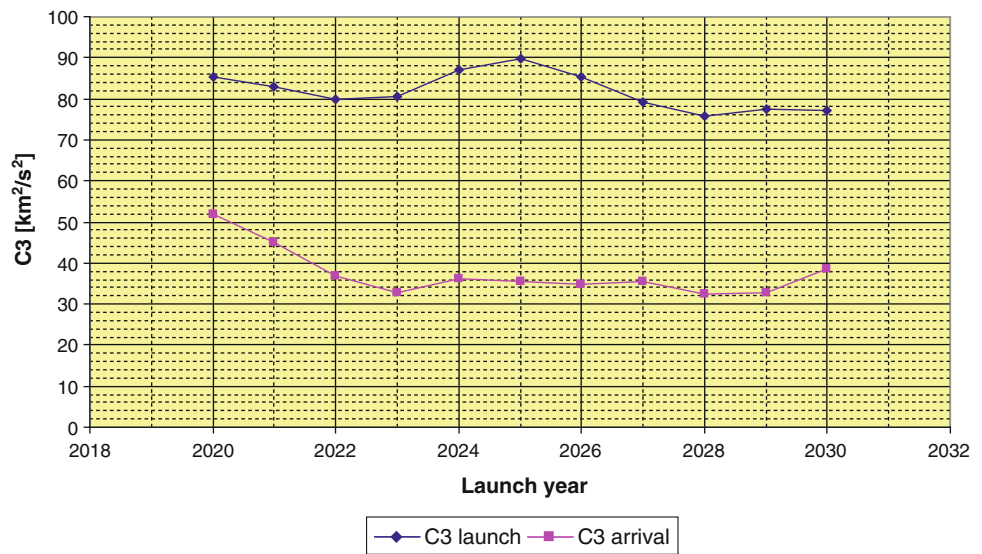


Figure 2.21 shows a typical Earth-Neptune transfer, constrained to 10 years transfer time.

2.3.8 Direct Transfer to Pluto

Table 2.13 shows the results for transfers to Pluto.

All transfers lead to extremely high C3's and high declinations. In fact, for launches in 2023–2030 all optimization results were not only constrained by the maximum transfer time of 10 years, but also the maximum escape declination of 51.8° . This constraint has a strong impact: the departure C3 is increasing rapidly. It is of little use re-optimizing these transfers for lower declination:

constraining the escape declination to 28.5° declination would lead to departure C3's of over $600 \text{ km}^2/\text{s}^2$.

Figure 2.22 shows the departure and arrival C3 in graphical form.

Figure 2.23 shows a typical Earth-Pluto trajectory, constrained to a transfer time of 10 years.

2.4 Avoiding Mars Dust Storms

In important aspect of missions to Mars is highlighted here: the fact that every two years a global dust storm appears on Mars. Typically the global dust storm season occurs for a solar longitude (the Mars-Sun angle, measured from the

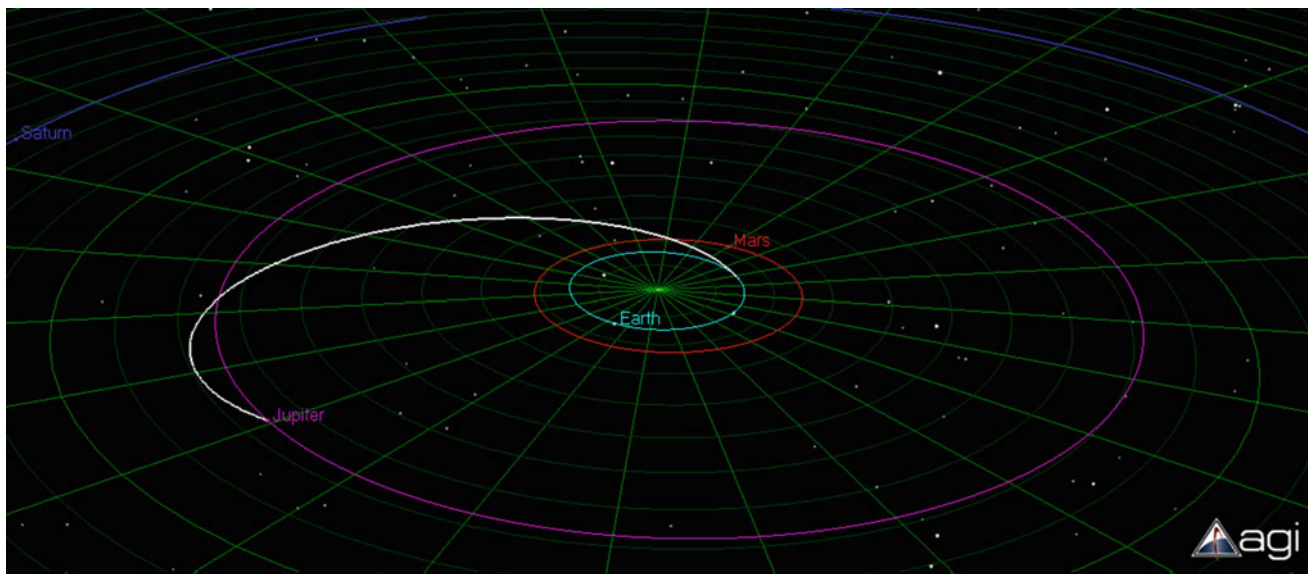


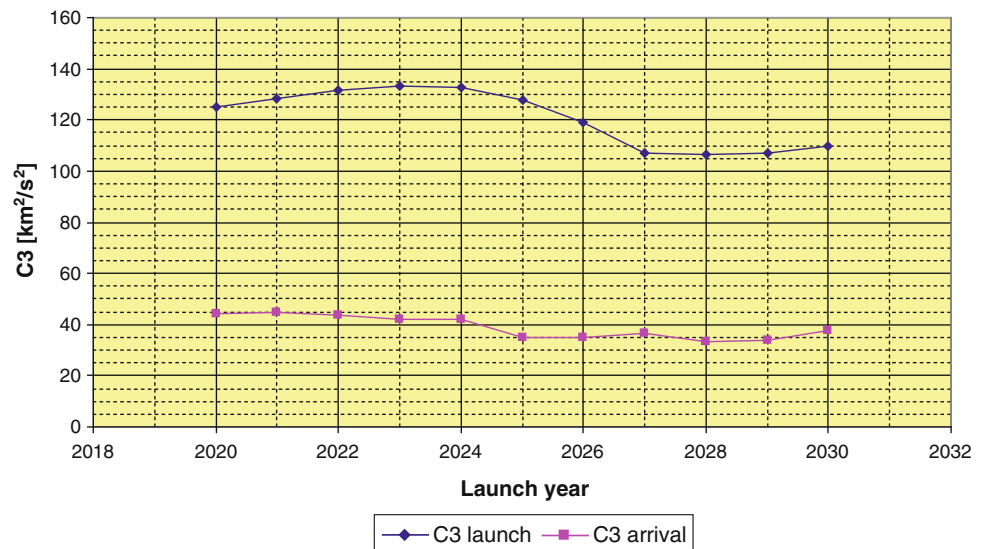
Fig. 2.15 Earth-Jupiter trajectory seen from a 3D perspective. Planet positions are shown at time of arrival

Table 2.9 Solutions for a direct transfer from Earth to Saturn

Year	Launch date	Arrival date	C3 launch [km^2/s^2]	C3 arrival [km^2/s^2]	Declination [$^\circ$]	Transfer time [yr]
2020	27-Mar-20	19-Oct-24	125.3	44.2	-44.6	4.56
2021	9-Apr-21	8-Oct-25	128.4	44.9	-46.3	4.50
2022	2-Apr-22	23-Oct-26	131.4	43.9	-46.0	4.56
2023	7-May-23	18-Nov-27	133.4	42.3	-44.3	4.53
2024	19-May-24	23-Nov-28	132.9	41.8	-40.9	4.51
2025	24-May-25	31-Oct-31	127.7	34.9	16.3	6.44
2026	10-Jun-26	31-Oct-32	119.1	34.9	16.9	6.39
2027	7-Jul-27	25-Apr-34	107.3	36.5	9.1	6.80
2028	14-Jul-28	22-Jun-34	106.5	33.1	8.2	5.94
2029	20-Jul-29	7-Jul-34	107.1	34.1	12.4	4.96
2030	4-Aug-30	7-Feb-35	110.0	37.9	22.0	4.51

Table 2.10 Solution for a direct transfer from Earth to Saturn, constrained to 28.5° launch declination and 7 years transfer time

Year	Launch date	Arrival date	C3 launch [km^2/s^2]	C3 arrival [km^2/s^2]	Declination [$^\circ$]	Transfer time [yr]
2020	18-Mar-20	18-Mar-27	145.0	32.6	4.9	7.00
2021	1-Apr-21	31-Mar-28	144.4	33.7	7.7	7.00
2022	15-Apr-22	14-Apr-29	141.1	34.9	9.5	7.00
2023	30-Apr-23	29-Apr-30	135.6	35.9	11.4	7.00
2024	15-May-24	15-May-31	128.4	36.7	13.1	7.00

Fig. 2.16 Departure and arrival C3 for a direct transfer from Earth to Saturn

Northern hemisphere spring equinox) from 180° to 340° . Table 2.14 gives an overview of when the typical dust storm seasons are in the 2020–2030 timeframe.

The year 2031 is also included since a launch in 2030 applies arriving in 2031. Typically one would not want to land a rover or take high resolution pictures of the surface when a dust storm is covering Mars, therefore these seasons are usually avoided. There are two ways to avoid this:

- Enter Mars orbit and wait in orbit until the storm is over
- Use an interplanetary trajectory that arrives after the storm

Often Mars landers are entering the Martian atmosphere immediately, without going into orbit first, so often the second approach is taken. It should be noted though that the dates in Table 2.14 are just predictions based on historical

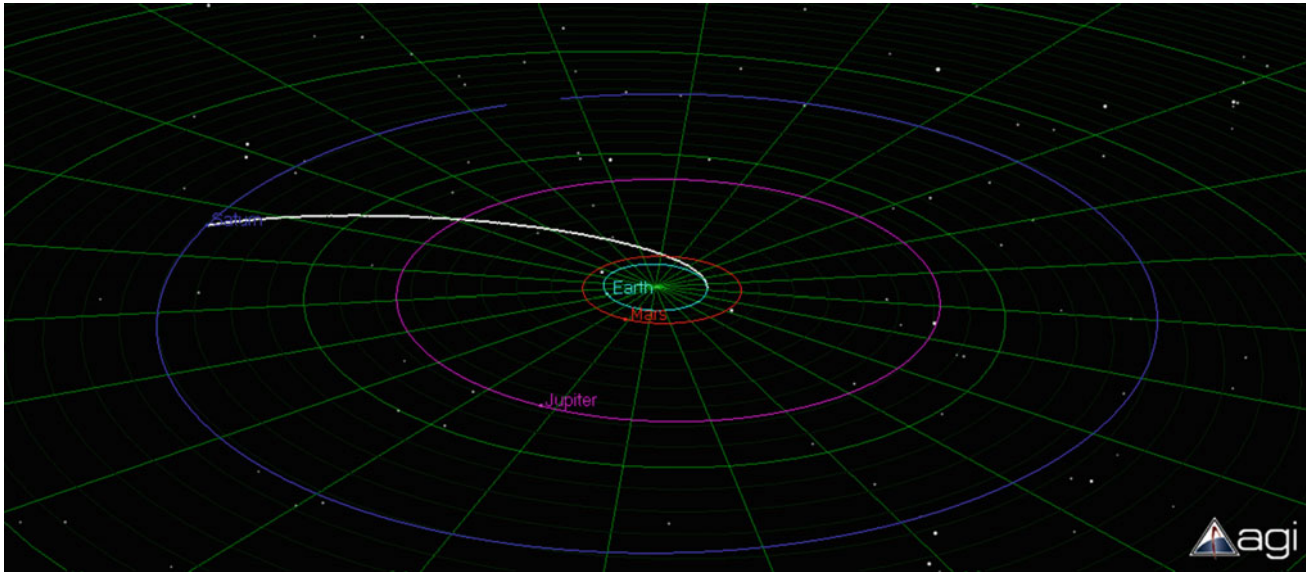
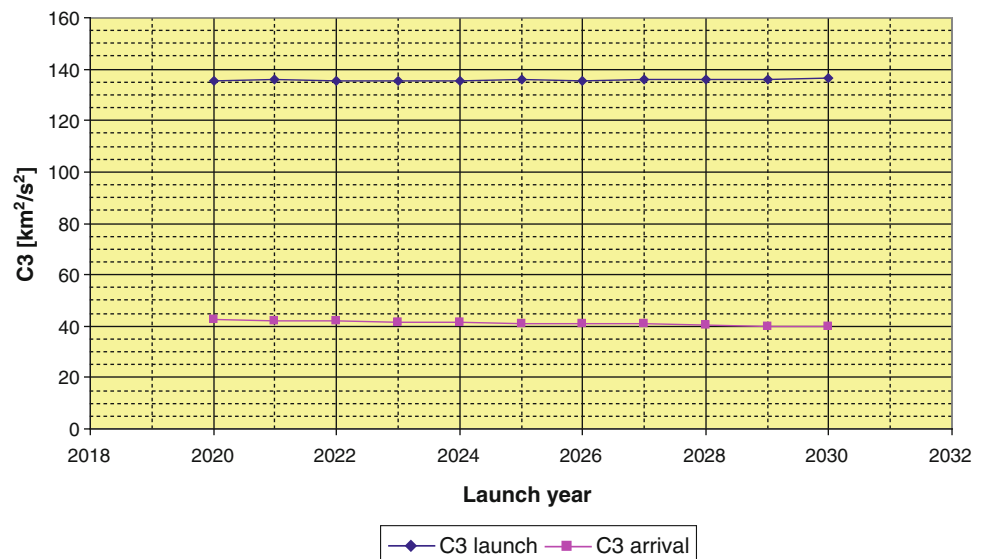


Fig. 2.17 Earth-Saturn trajectory seen from a 3D perspective. Planet positions are shown at time of arrival

Table 2.11 Solutions for a direct transfer from Earth to Uranus

Year	Launch date	Arrival date	C3 launch [km^2/s^2]	C3 arrival [km^2/s^2]	Declination [$^\circ$]	Transfer time [yr]
2020	22-Jun-20	22-Jun-30	135.2	42.6	1.4	10.00
2021	27-Jun-21	27-Jun-31	135.7	42.2	3.8	10.00
2022	1-Jul-22	30-Jun-32	135.2	41.9	6.5	10.00
2023	7-Jul-23	6-Jul-33	135.6	41.6	8.4	10.00
2024	10-Jul-24	10-Jul-34	135.3	41.4	11.3	10.00
2025	15-Jul-25	15-Jul-35	135.7	41.1	13.7	10.00
2026	20-Jul-26	19-Jul-36	135.6	40.9	15.9	10.00
2027	25-Jul-27	24-Jul-37	135.9	40.7	18.3	10.00
2028	29-Jul-28	29-Jul-38	136.0	40.4	20.5	10.00
2029	4-Aug-29	4-Aug-39	136.1	40.0	21.9	10.00
2030	8-Aug-30	7-Aug-40	136.5	39.7	24.8	10.00

Fig. 2.18 Departure and arrival C3 for a direct transfer from Earth to Uranus



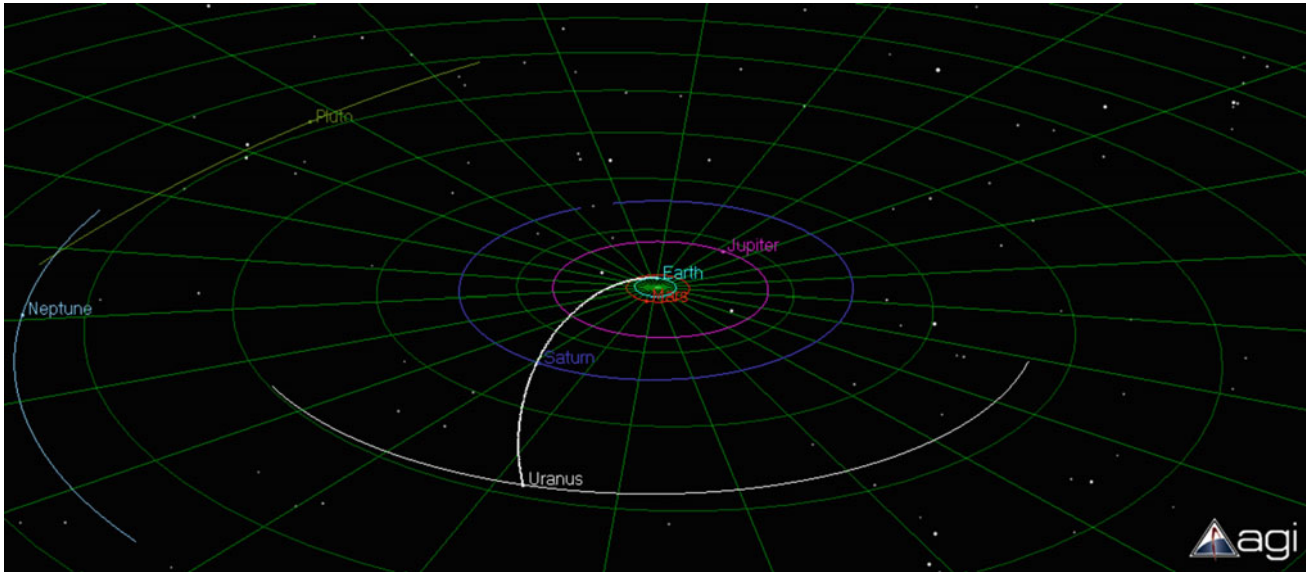
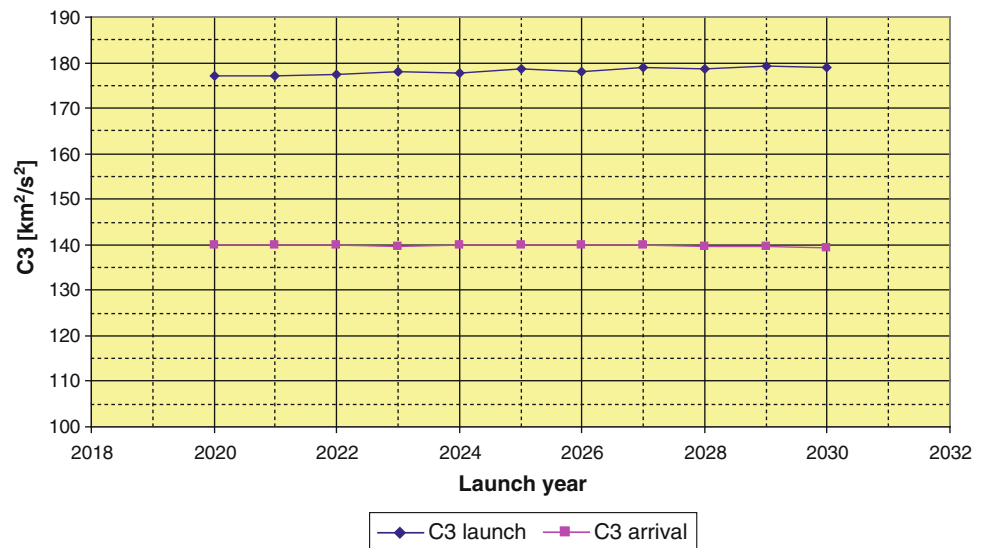


Fig. 2.19 Earth-Uranus trajectory, constrained to 10 years transfer time, seen from a 3D perspective. Planet positions are shown at time of arrival

Table 2.12 Solutions for a direct transfer from Earth to Neptune

Year	Launch date	Arrival date	C3 launch [km^2/s^2]	C3 arrival [km^2/s^2]	Declination [$^\circ$]	Transfer time [yr]
2020	2-May-20	2-May-30	177.20	140.00	-26.30	10.00
2021	6-May-21	6-May-31	177.20	140.00	-25.70	10.00
2022	7-May-22	6-May-32	177.50	139.80	-25.30	10.00
2023	11-May-23	10-May-33	177.90	139.70	-24.70	10.00
2024	12-May-24	12-May-34	177.80	139.90	-24.20	10.00
2025	15-May-25	15-May-35	178.50	139.90	-23.60	10.00
2026	17-May-26	16-May-36	178.10	139.90	-23.00	10.00
2027	20-May-27	19-May-37	179.00	139.80	-22.30	10.00
2028	21-May-28	21-May-38	178.50	139.70	-21.60	10.00
2029	23-May-29	23-May-39	179.20	139.50	-20.90	10.00
2030	27-May-30	26-May-40	178.90	139.20	-20.20	10.00

Fig. 2.20 Departure and arrival C3 for a direct transfer from Earth to Neptune



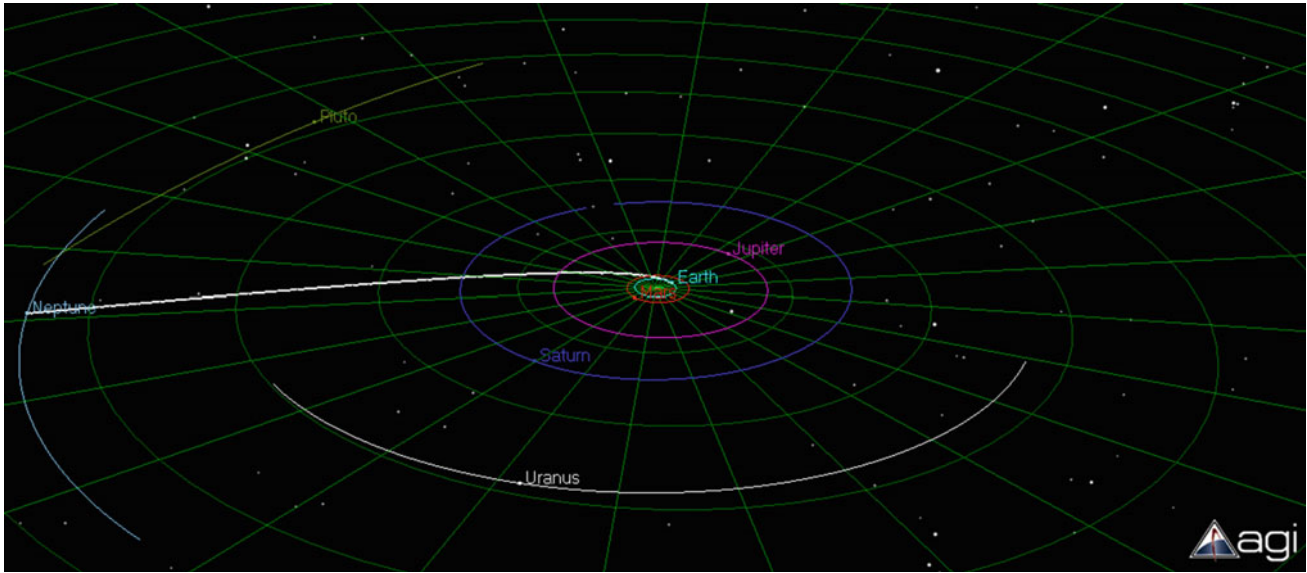


Fig. 2.21 Earth-Neptune trajectory, constrained to 10 years transfer time, seen from a 3D perspective. Planet positions are shown at time of arrival

Table 2.13 Solutions for a direct transfer from Earth to Pluto

Year	Launch date	Arrival date	C3 launch [km^2/s^2]	C3 arrival [km^2/s^2]	Declination [$^\circ$]	Transfer time [yr]
2020	14-Mar-20	14-Mar-30	235.70	201.00	-47.20	10.00
2021	16-Mar-21	16-Mar-31	241.20	204.80	-49.00	10.00
2022	19-Mar-22	18-Mar-32	247.80	208.60	-50.20	10.00
2023	21-Mar-23	20-Mar-33	253.10	212.60	-51.80	10.00
2024	25-Mar-24	25-Mar-34	261.10	216.30	-51.50	10.00
2025	29-Mar-25	29-Mar-35	268.30	220.00	-51.70	10.00
2026	2-Apr-26	1-Apr-36	278.00	223.60	-51.70	10.00
2027	6-Apr-27	5-Apr-37	287.20	227.20	-51.70	10.00
2028	9-Apr-28	9-Apr-38	298.90	230.80	-51.60	10.00
2029	13-Apr-29	13-Apr-39	310.40	234.40	-51.40	10.00
2030	16-Apr-30	15-Apr-40	320.50	238.30	-51.70	10.00

data. The dust storm could easily start a month later. However the dates contain margins so we take them as a reference.

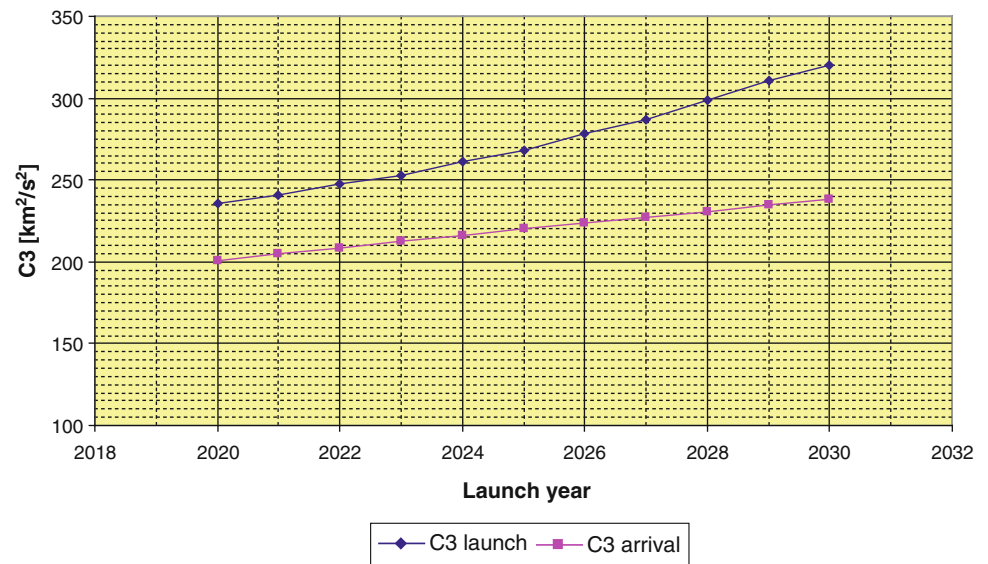
Looking at Table 2.6, we see that there are transfers with arrivals in or just before the dust storm season. The 2026 transfer is an example: the arrival time is 3 September 2027 and the dust storm season starts in 18 October 2027. The same applies to the 2028 and 2030 launches. For these transfers, we would prefer to arrive after the dust storm season (5 July 2028, 23 May 2030 and 9 April 2032 respectively). Typically this is done by following a full orbit around the Sun at least once before arriving at Mars.

Table 2.15 gives an overview of transfers for 2026, 2028 and 2030 with the constraint to arrive after the dust storm season.

Figure 2.24 shows a typical Earth-Mars transfer with an arrival date after the dust storm.

The USA launched the Mariner 9 mission (see Fig. 2.25) on 30 May 1970 by an Atlas rocket. It arrived at Mars on 14 November in the same year. It became the first spacecraft to orbit another planet however after it entered Mars orbit, Mars was covered with clouds and the pictures did not reveal any feature of the surface. After months of waiting, the storm finally disappeared and the 560 kg spacecraft started the first

Fig. 2.22 Departure and arrival C3 for a direct transfer from Earth to Pluto



global mapping of Mars, revealing many features such as details on the largest volcano in the Solar System: Olympus Mons (see Fig. 2.26).

2.5 Return Missions

Sometimes a return leg from the planet back to Earth is required. This is the case for example for sample return missions. These missions are extremely complex and require a very large launch mass since an entire launcher needs to be

Table 2.14 Overview of Mars global dust storm seasons

Dust storm season start [Ls = 180°]	Dust storm season ends [Ls = 340°]
9 April 2020	26 December 2020
25 February 2022	13 November 2022
13 January 2024	30 September 2024
30 November 2025	18 August 2026
18 October 2027	5 July 2028
4 September 2029	23 May 2030
23 July 2031	9 April 2032

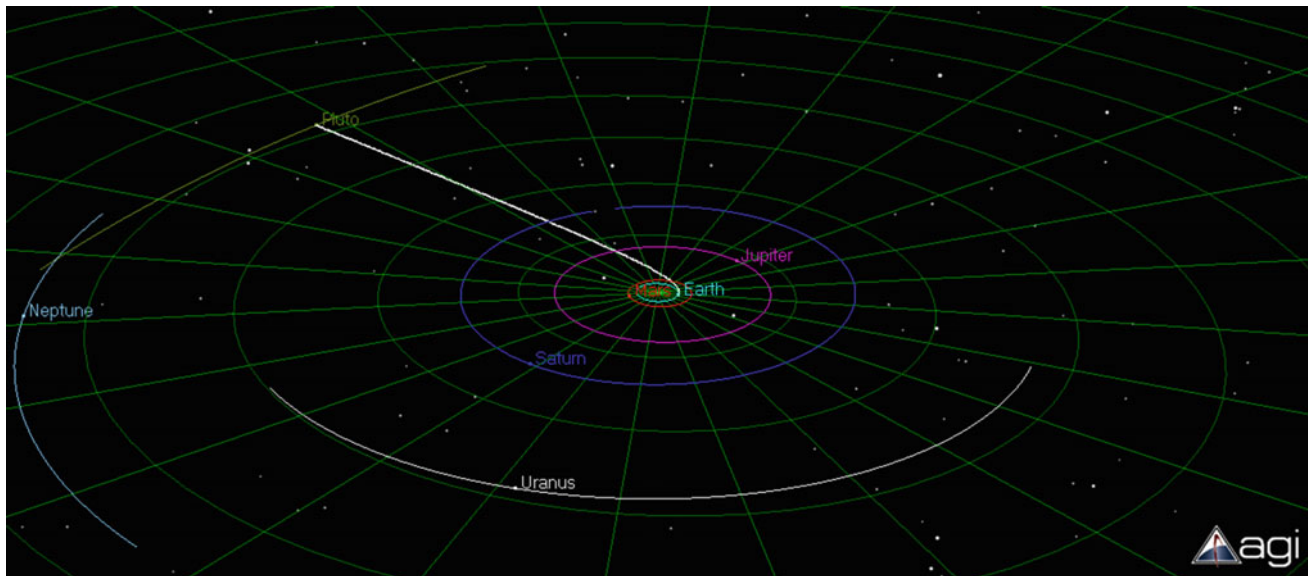


Fig. 2.23 Earth-Pluto trajectory, constrained to 10 years transfer time, seen from a 3D perspective. Planet positions are shown at time of arrival

Table 2.15 Solutions for a direct transfer from Earth to Mars, arriving after dust storms

Year	Launch date	Arrival date	C3 launch [km^2/s^2]	C3 arrival [km^2/s^2]	Declination [$^\circ$]	Transfer time [yr]
2026	5-Jul-26	5-Jul-28	11.5	8.2	10.5	2.00
2028	12-Sep-28	24-Mar-31	13.4	7.1	10.3	2.53
2030	28-Sep-30	5-Mar-33	11.6	6.1	14.7	2.43

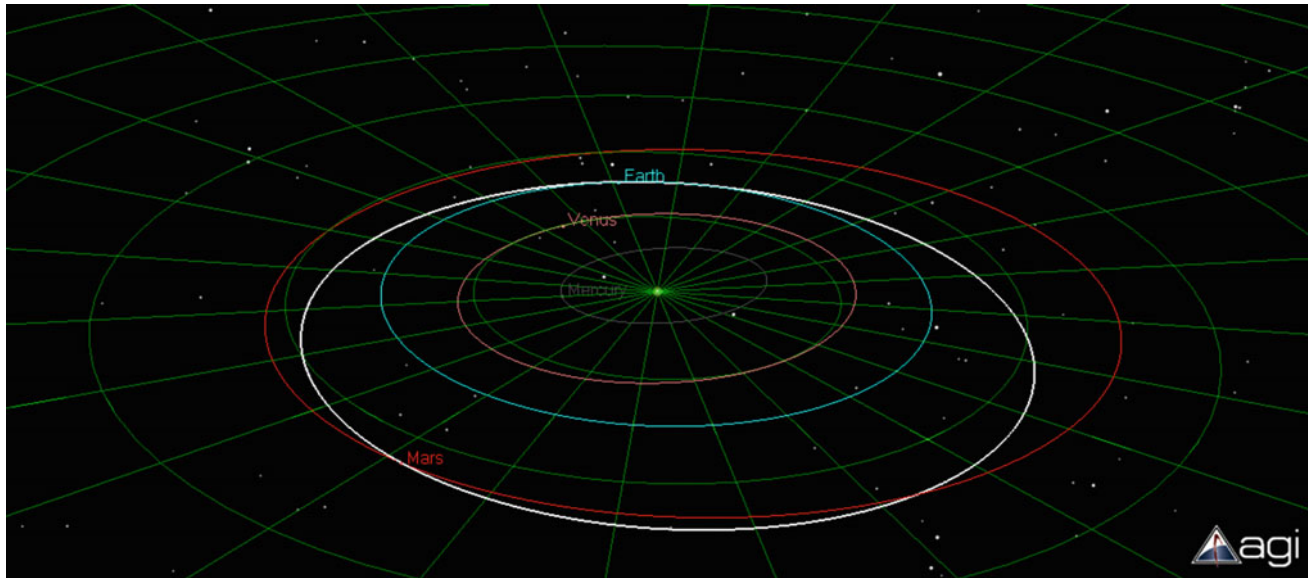
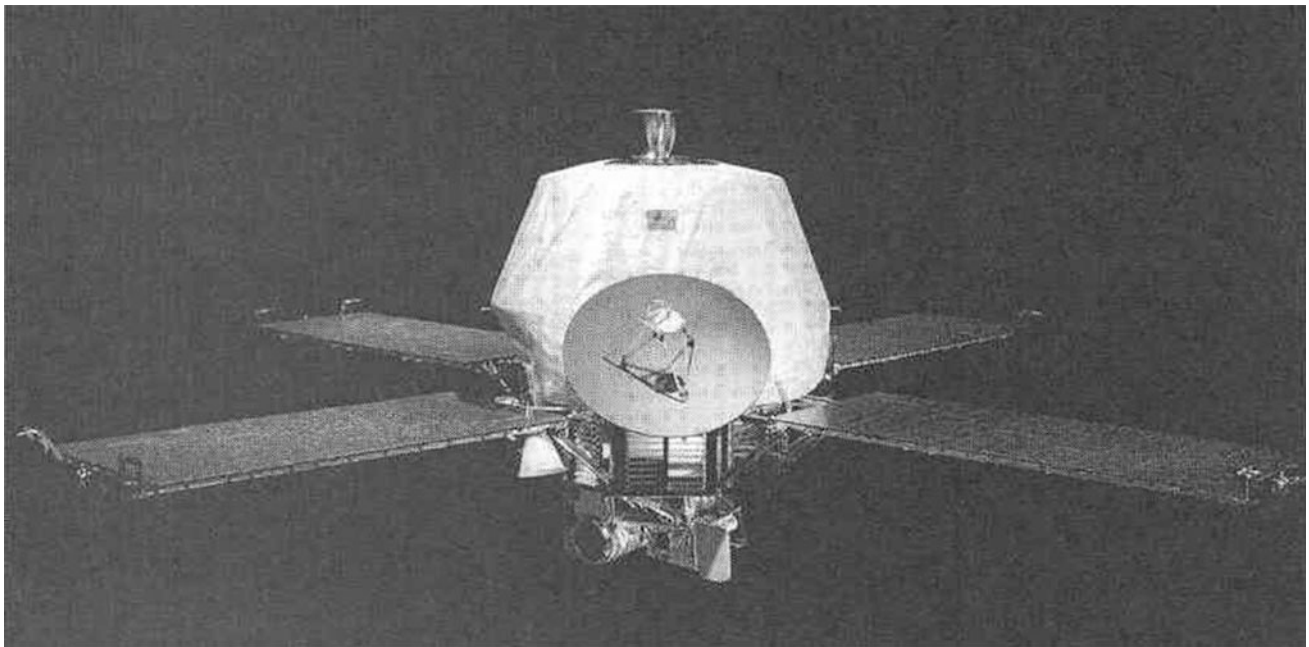
**Fig. 2.24** Earth-Mars trajectory using one complete heliocentric orbit, constrained to arrive after a dust storm, seen from a 3D perspective. Planet positions are shown at time of arrival**Fig. 2.25** Mariner 9 spacecraft overview. *Credits NASA*

Fig. 2.26 Mariner 9 picture of Olympus Mons, sticking out above the dust storms. Credits NASA



Table 2.16 Solutions for a return transfer from Venus to Earth

Year	Launch date	Arrival date	C3 launch [km^2/s^2]	C3 arrival [km^2/s^2]	Transfer time [yr]
2020	3-Jun-21	8-Sep-22	28.8	9.9	1.26
2021	2-Dec-21	22-Mar-22	24.6	9.2	0.30
2023	24-Jan-25	4-Jun-25	8.2	9.0	0.36
2024	27-Jul-26	24-Dec-26	17.8	9.0	0.41
2026	6-Mar-28	2-Sep-28	26.1	9.6	0.49
2028	27-Nov-29	21-Mar-30	24.1	9.7	0.31

put on the other planet. Studies have been performed for Venus Sample Return and Mars Sample Return missions, so this section will show return legs for these two planets. A constraint is that the return leg should start after the Earth-to-planet arrival date. Another constraint often applied is the arrival infinite velocity (and therefore the Earth arrival C3). This has to do with the maximum heat flux that the Thermal Protection System can handle. Often the arrival C3 is constrained to be below $10 \text{ km}^2/\text{s}^2$. Also, there is no final orbit; a direct entry into the Earth's atmosphere is assumed. Table 2.16 gives an overview of possible Venus-Earth return legs for launches (from Earth) in the 2020–2030 timeframe.

The first return leg (2020 launch) follows a complete heliocentric orbit around the Sun before returning to Earth, and actually arrives later than the return leg shown for the 2021 launch. The first row is therefore to highlight possible transfers. If the satellite is launched to Venus in 2020, it

could leave Venus in June 2021 (and only arrive at Earth in September 2022) or wait a bit and leave in December 2021, and arrive earlier (March 2022). Figure 2.27 shows a typical Venus-Earth transfer.

Table 2.17 shows an overview of possible Mars-Earth return legs for launches (from Earth) in the 2020–2030 timeframe.

And Fig. 2.28 shows a typical Mars-Earth transfer.

The Russian Federal Space Agency launched the Phobos-Grunt spacecraft on 9 November 2011 using a Zenith launcher, to become the first interplanetary sample return mission. Its objective was to capture a sample from Mars' moon Phobos, and return it to Earth. Figure 2.29 shows the mission profile.

Phobos-Grunt was one of the most complex robotic mission designs ever, with the spacecraft consisting of four stages as shown in Fig. 2.30. First, a bi-propellant propulsion

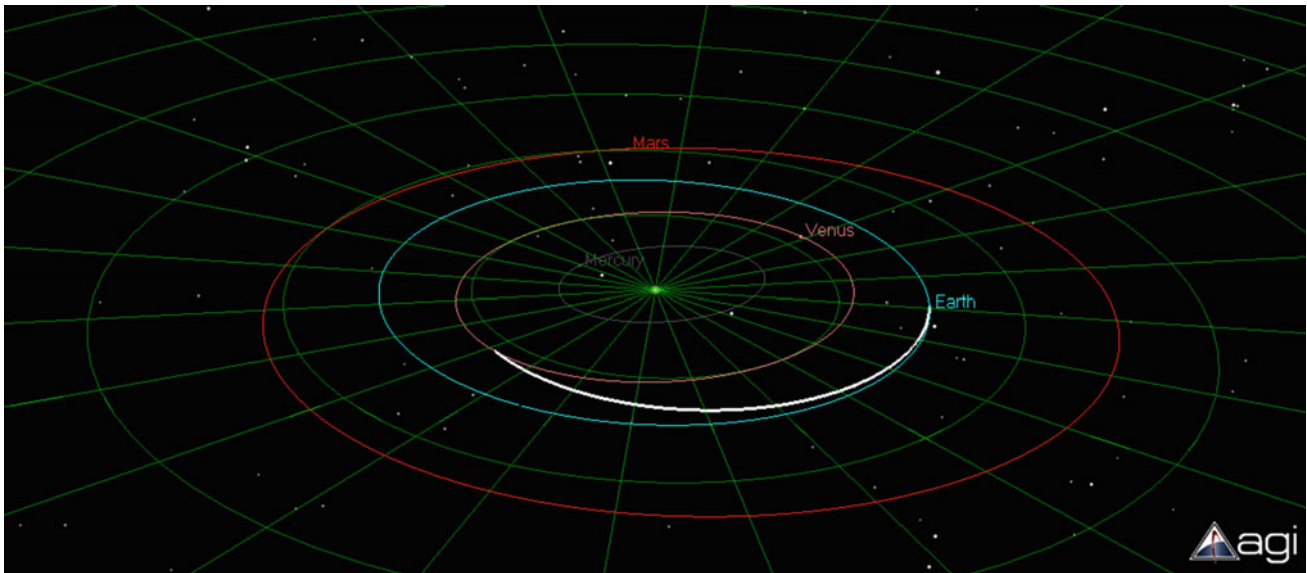


Fig. 2.27 Venus-Earth trajectory, seen from a 3D perspective. Planet positions are shown at time of arrival

Table 2.17 Solutions for a return transfer from Mars to Earth

Year	Launch date	Arrival date	C3 launch [km^2/s^2]	C3 arrival [km^2/s^2]	Transfer time [yr]
2020	18-Jul-22	17-Apr-23	11.4	9.8	0.75
2022	27-Jul-24	12-May-25	8.6	7.9	0.79
2024	31-Jul-26	17-Jun-27	7.2	9.4	0.88
2026	17-Mar-30	10-May-32	8.6	7.8	2.15
2028	3-Mar-32	27-May-34	7.5	8.6	2.23
2030	23-Feb-34	21-Jun-36	7.0	9.9	2.32

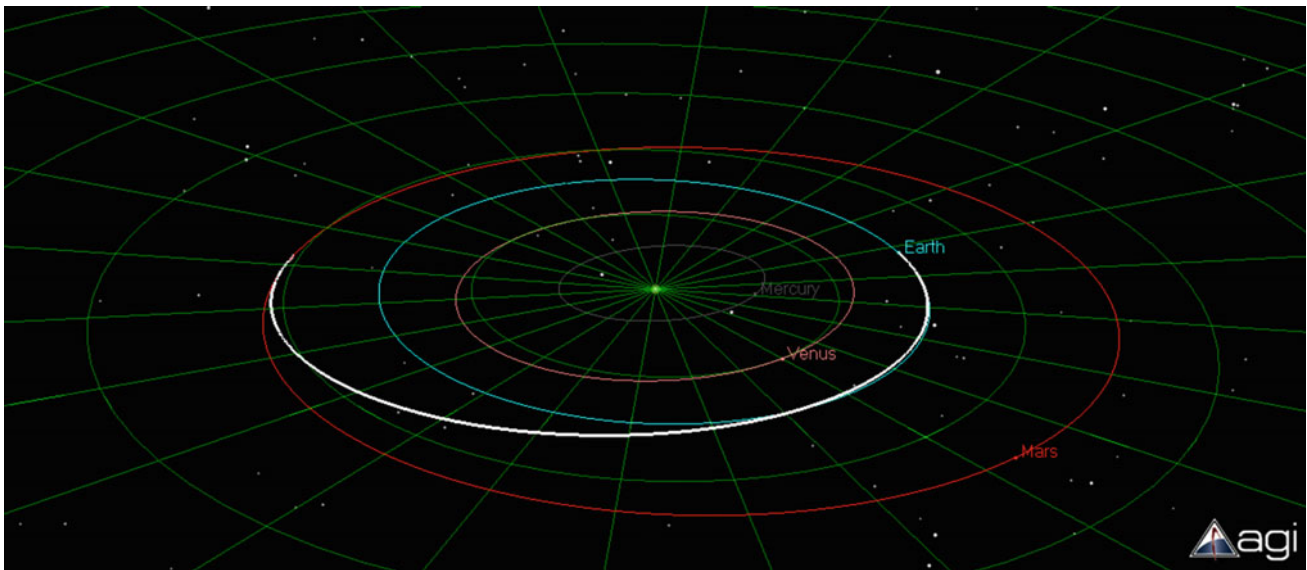


Fig. 2.28 Mars-Earth trajectory, seen from a 3D perspective. Planet positions are shown at time of arrival

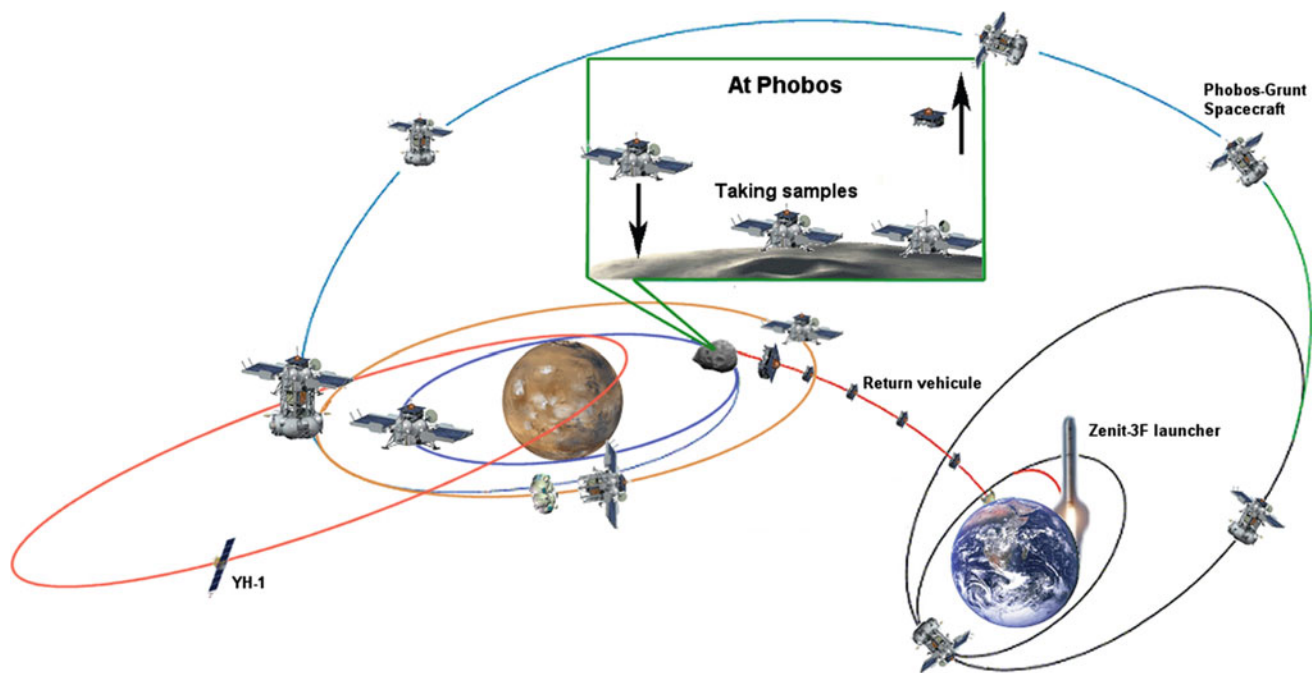
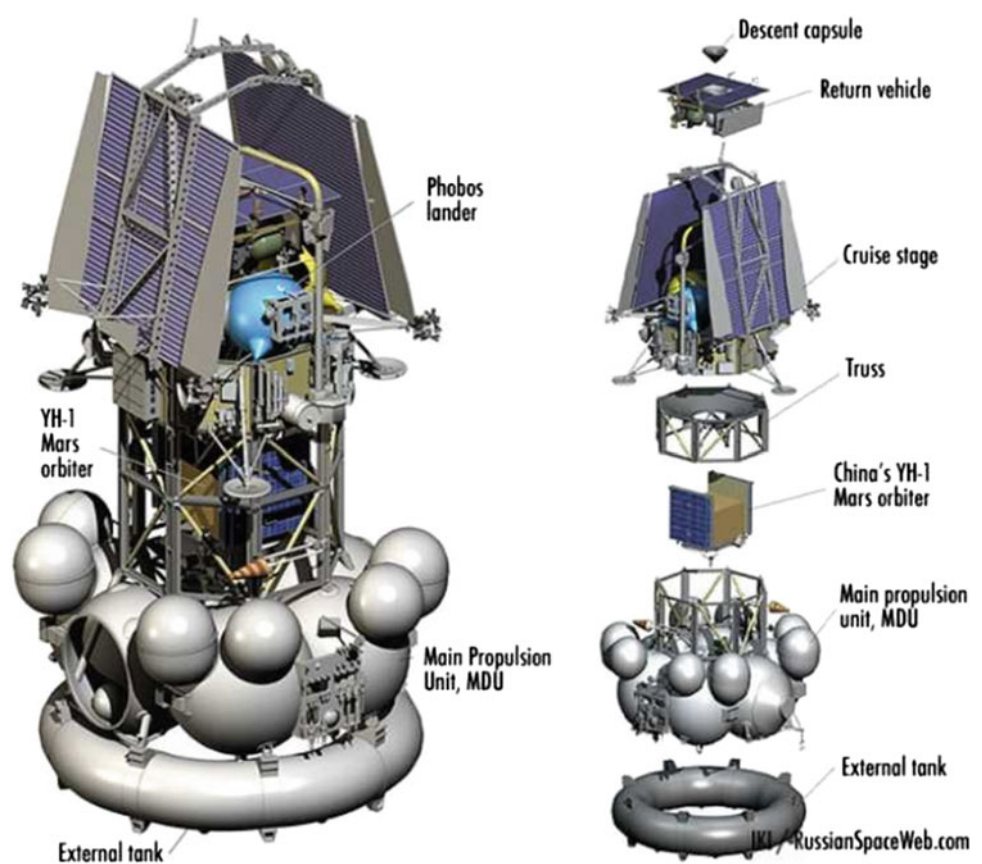


Fig. 2.29 Phobos-Grunt return trajectory overview. *Credits Roscosmos*

Fig. 2.30 Phobos-Grunt in launch configuration showing, from *top* to *bottom*, the descent capsule (4th stage), the ERC (3rd stage), the lander/cruise stage (2nd stage) and the propulsion module (1st stage) with its extra toroid-shaped external tank. *Credits Roscosmos*



stage, derived from Soyuz's Fregat upper-stage, was used to escape the Earth from LEO. The escape was done using a sequence of maneuvers. Half-way this procedure, a toroid-shaped propellant tank was ejected. Mars orbit insertion was performed using the same propulsions stage, which was then ejected. The second stage was the Phobos lander which contained a propulsion system to land on the surface. It also contained the power system, communications system and robotic arms to sample the soil of Phobos. The third stage was the Earth Return Capsule (ERC) that again contained a propulsion system, this time used to not only ascent from the surface of Phobos (which would put the system into Mars orbit), but also to escape from Mars. This third stage was again a satellite on its own, carrying solar panels and a communication system. The fourth and final stage was the Descent Stage: a small capsule containing the samples that were transferred into this capsule from the lander using tubes. The near-spherical stage was covered with a Thermal Protection System (TPS) to withstand the heat fluxes during Earth re-entry. Unfortunately, like roughly half of the missions to Mars, Phobos-Grunt ended up in mission failure, as the first stage failed to ignite.

2.6 Examples

2.6.1 Mission to Mars

Exercise: calculate the maximum satellite mass on-board Falcon-9 for a launch to Mars in 2026. Also estimate the launch mass applicable to a three-week launch window. The mission is to avoid dust re-entrystorms.

Result: from Table 2.15 we find that the C3 for a launch in 2026 is: $11.5 \text{ km}^2/\text{s}^2$.

Then, from Fig. 1.18, we find the launcher performance: 1800 kg. In Sect. 2.3 it was suggested to reduce the optimal

launch mass by 1.5 % in order to estimate the lowest mass during the launch window. Therefore, the mass applicable to the launch window is: $1800 \text{ kg} - 1.5 \% = 1773 \text{ kg}$.

2.6.2 Mission to Neptune

Exercise: is there a launcher capable of launching a satellite to Neptune in the 2020–2030 timeframe, using a direct transfer?

Result: from Table 2.12 we see that the highest C3 found is $179 \text{ km}^2/\text{s}^2$. The two heavy-lift launchers Ariane 5 and Proton-M (see Figs. 1.14 and 1.17) show that no numbers exist for this C3. Even using a parking orbit, as shown in Sect. 1.10, does not show numbers higher from a C3 of $100 \text{ km}^2/\text{s}^2$. The reason is that it becomes impossible to perform a trajectory burn to reach such C3, without taking an amount of time well beyond the qualified thrust durations of the engine. Atlas V shows a low performance ($\pm 275 \text{ kg}$) for this C3. For a satellite going that far away from Earth and Sun, and therefore requiring a large antenna, special systems for power generation etc., this is a very challenging mass constraint. An alternative method should be sought, such as using a trajectory based on one or more swing-bys (a trajectory using Jupiter as a swing-by planet should be close to the C3 required for a direct transfer to Jupiter, i.e. $85 \text{ km}^2/\text{s}^2$, which would divide the launch C3 in half), or leaving with low C3 and use Deep-Space Maneuvers performed by, for example, a low-thrust engine.

References

1. "Solar System Dynamics", NASA, <http://ssd.jpl.nasa.gov/?horizons>
2. "Systems Tool Kit", AGI, <http://www.agi.com/products/stk/>

<http://www.springer.com/978-3-319-26981-8>

Lunar and Interplanetary Trajectories

Biesbroek, R.

2016, XV, 227 p. 320 illus., 292 illus. in color.,

Hardcover

ISBN: 978-3-319-26981-8